

Mechanics and remodelling of cell packings in epithelia

D.B. Staple¹, R. Farhadifar¹, J.-C. Röper², B. Aigouy², S. Eaton², and F. Jülicher^{1,a}

¹ Max Planck Institute for the Physics of Complex Systems, Nöthnitzerstrasse 38, 01187 Dresden, Germany

² Max Planck Institute of Molecular Cell Biology and Genetics, Pfotenhauerstrasse 108, 01307 Dresden, Germany

Received 14 June 2010 and Received in final form 7 October 2010

Published online: 17 November 2010 – © EDP Sciences / Società Italiana di Fisica / Springer-Verlag 2010

Abstract. Epithelia are sheets of cells that are dynamically remodelled by cell division and cell death during development. Here we describe the cell shapes and packings as networks of polygons: stable and stationary network configurations obey force balance and are represented as local minima of a potential function. We characterize the physical properties of this vertex model, including the set of ground states, and the energetics of topological rearrangements. We furthermore discuss a quasistatic description of cell division that allows us to study the mechanics and dynamics of tissue remodelling during growth. The biophysics of cells and their rearrangements can account for the morphology of cell packings observed in experiments.

1 Introduction

During the development of an organism from a fertilized egg, cells multiply by cell division and organize in multicellular arrangements. An important situation is the formation of epithelia, which are sheet-like two-dimensional packings of cells. An epithelium defines a surface that divides space into two regions, the basal and the apical side. The cells in the epithelium exhibit an apical-basal asymmetry. Close to the apical side, cell contacts form highly organized adherens junctions: these junctions are enriched in adhesion molecules and are associated with bundles of cortical actin and myosin in the adjacent cells. This network of adherens junctions organizes the morphology of cell packings, guides cell rearrangements, and defines the geometry of cell packings. Remarkably, some of the detailed structure of epithelia (*e.g.* polygon distributions) can be understood using topological arguments alone [1,2]. Nevertheless, understanding the mechanics and dynamics of development at the cell scale demands a theoretical treatment of tissue mechanics.

During development, epithelial tissues are dynamically remodelled. Remodelling involves topological changes of the junctional network, induced, for example, by cell division, cell extrusion, and cell boundary rearrangement. Extrusion implies that cells undergo apoptosis and leave the epithelium. As a consequence, over time scales of hours and days, a developing epithelium undergoes dramatic reorganization and patterning processes. Such dynamic reorganization of epithelia can be studied experimentally in model systems. An important system is the development of the fly wing from a precursor structure, the wing

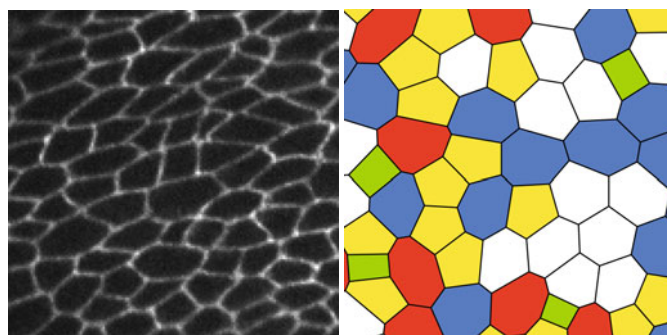


Fig. 1. (a, left) Confocal microscope image of a developing *Drosophila* wing (E-cadherin labelled with green fluorescent protein in a wing disc epithelium). (b, right) Epithelia in the vertex model are represented as networks of polygons.

imaginal disc, which consists of two epithelial layers. The network of adherens junctions of an epithelium can be observed experimentally, see fig. 1a. Its reorganization is governed by force balance and the biophysical properties of cells and their adhesive contacts. A physical description of tissue organization and mechanics can thus be based on the mechanics of the junctional network [3].

Tissue morphology can be described by vertex models, which account for the geometry of the junctional network using polygons. These polygons are characterized by the positions of vertices and linear bonds connecting them, see fig. 1b. Force balance in the junctional network is described using a potential or work function. Such vertex models are a coarse-grained representation of cell shape and thus do not capture finer details such as curvature of bonds. Vertex models have been used to discuss tissue

^a e-mail: julicher@pks.mpg.de

morphology [4], dynamics [5,6], and, more recently, to study detailed problems such as the dynamics of wound closure [7], cell sorting [8], the mechanical regulation of cell division and growth [9], and the emergence and reorientation of planar polarity [10]. Early models were evoked in discussions of foam [11–15] and grain boundaries [16,17] rather than living tissue, and this parallel continues today [18]. We have recently presented a vertex model that can account for the geometry of the junctional network in the wing disc (epithelium that forms the developing wing) of the fruit fly *Drosophila* [3]. We determined biophysical parameters that describe the properties of cell mechanics and adhesion, showing that this vertex model can quantitatively account for the observed statistical properties of cell packings and that irregularities in the packings result largely from stochastic cell division.

Vertex models can be made computationally efficient in two dimensions, however it is not straightforward to generalize vertex models to three dimensions. An important method has been to use a modification of the many-states Potts model [19–21] in order to represent complex cell shapes in two and three dimensions. A slightly different approach is to treat cells exclusively using cell-centers (see [22] and references therein); such calculations are typically less detailed but more computationally efficient. Tissues have been recently treated on large length scales using continuum descriptions [23–25]. Similar models have also been used to study wound closure [26] and the geometric structure of ommatidia in the *Drosophila* eye [27].

The broad relevance of vertex models for cell mechanics in different systems demands a detailed understanding of these models. In this paper, we systematically explore the physical properties of a vertex model using analytic arguments and high-precision simulations. Our results extend and refine those presented in [3]. We briefly review the vertex model in sect. 2. We discuss in sect. 3 the ground states of the model and present a ground-state diagram. In sect. 4 we discuss general elastic properties of ground states, in particular the compression and shear moduli. The energetics of topological rearrangements of the network by T1 and T2 transitions are discussed in sect. 5. Based on the force balance described by the vertex model, we discuss in sect. 6 a quasistatic description of cell division that can be used to study the mechanics and morphology of tissue growth. The article concludes with a discussion of what has been achieved and future directions.

2 Vertex model for cell shape and tissue mechanics

The geometry of the polygonal network is described by a set of vertex positions \mathbf{r}_i , with $i = 1, \dots, N_V$, where N_V denotes the number of vertices, together with N_B bonds $\langle i, j \rangle$ that connect vertices i and j . Each polygon describes one cell, indexed by $\alpha = 1, \dots, N$, where N is the number of cells in the system. The mechanical properties of the network in stationary conditions are described

by a potential or work function

$$F(\mathbf{r}_i) = \sum_{\alpha} \frac{K_{\alpha}}{2} (A_{\alpha} - A_{\alpha}^{(0)})^2 + \sum_{\langle i, j \rangle} \Lambda_{ij} l_{ij} + \sum_{\alpha} \frac{\Gamma_{\alpha}}{2} L_{\alpha}^2. \quad (1)$$

Here, A_{α} denotes the area of cell α , L_{α} is the cell perimeter and l_{ij} is the length of bond $\langle i, j \rangle$. The first term describes area elasticity, where the sum is over all cells α . If the polygonal area A_{α} of a cell with constant volume $V = A_{\alpha}h$ is changed, the cell height h adjusts. Under such a deformation the elastic energy can be described by an area elastic modulus K_{α} and a preferred area $A^{(0)}$. The second term describes bond tension Λ_{ij} , where the sum is over all bonds $\langle i, j \rangle$. This tension results from actomyosin contractility in the cortical bundles associated with the adherens junctions, and also from the mechanics of cell-cell adhesion. In a general expansion of the work function in terms of geometrical properties, the next-order term is quadratic in bond length. We introduce as a specific choice of a quadratic term the perimeter elasticity described by the coefficient Γ_{α} . This term accounts for changes in bond tension due to a change in cell perimeter. It is motivated by the fact that an actomyosin ring underlies the adherens junctional network, which is in general expected to exert a tension depending on cell perimeter.

3 Ground states of the vertex model

Here we systematically determine the ground states of the vertex model. Ground states can be interpreted as being the most relaxed network configurations. They are the absolute minima of F for a given number of cells N , using periodic boundary conditions for simplicity. The size of the periodic box is given by the lengths L_x and L_y . We consider the case where all cells have the same properties, *i.e.*, they all have a common preferred area $A_{\alpha}^{(0)} = A_0$, perimeter stiffness $\Gamma_{\alpha} = \Gamma$, area stiffness $K_{\alpha} = K$, and all bonds have the same line tension $\Lambda_{ij} = \Lambda$. The dimensionless potential energy per cell $\bar{F} = F/(NKA_0^2)$ can be written as

$$\bar{F} = \frac{1}{N} \sum_{\alpha} e(a_{\alpha}, p_{\alpha}), \quad (2)$$

with

$$e(a, p) = \frac{1}{2} [(a - 1)^2 + \bar{\Gamma}(p - p_0)^2] + e_0, \quad (3)$$

where $a_{\alpha} = A_{\alpha}/A_0$ and $p_{\alpha} = L_{\alpha}/\sqrt{A_0}$. The model parameters are represented as $p_0 = -\bar{\Lambda}/2\bar{\Gamma}$, which is a dimensionless preferred perimeter and $e_0 = -\bar{\Lambda}^2/8\bar{\Gamma}$, where $\bar{\Lambda} = \Lambda/(KA_0^{3/2})$ and $\bar{\Gamma} = \Gamma/(KA_0)$. In writing eq. (3) we have made use of the choice that all bonds have the same line tension $\Lambda_{ij} = \Lambda$, so that line tension can be absorbed in the perimeter term by introducing p_0 . Changes in area δa and perimeter δp imply a change in potential,

$$\delta e = (a - 1)\delta a + \bar{\Gamma}(p - p_0)\delta p + \frac{1}{2}(\delta a^2 + \bar{\Gamma}\delta p^2). \quad (4)$$

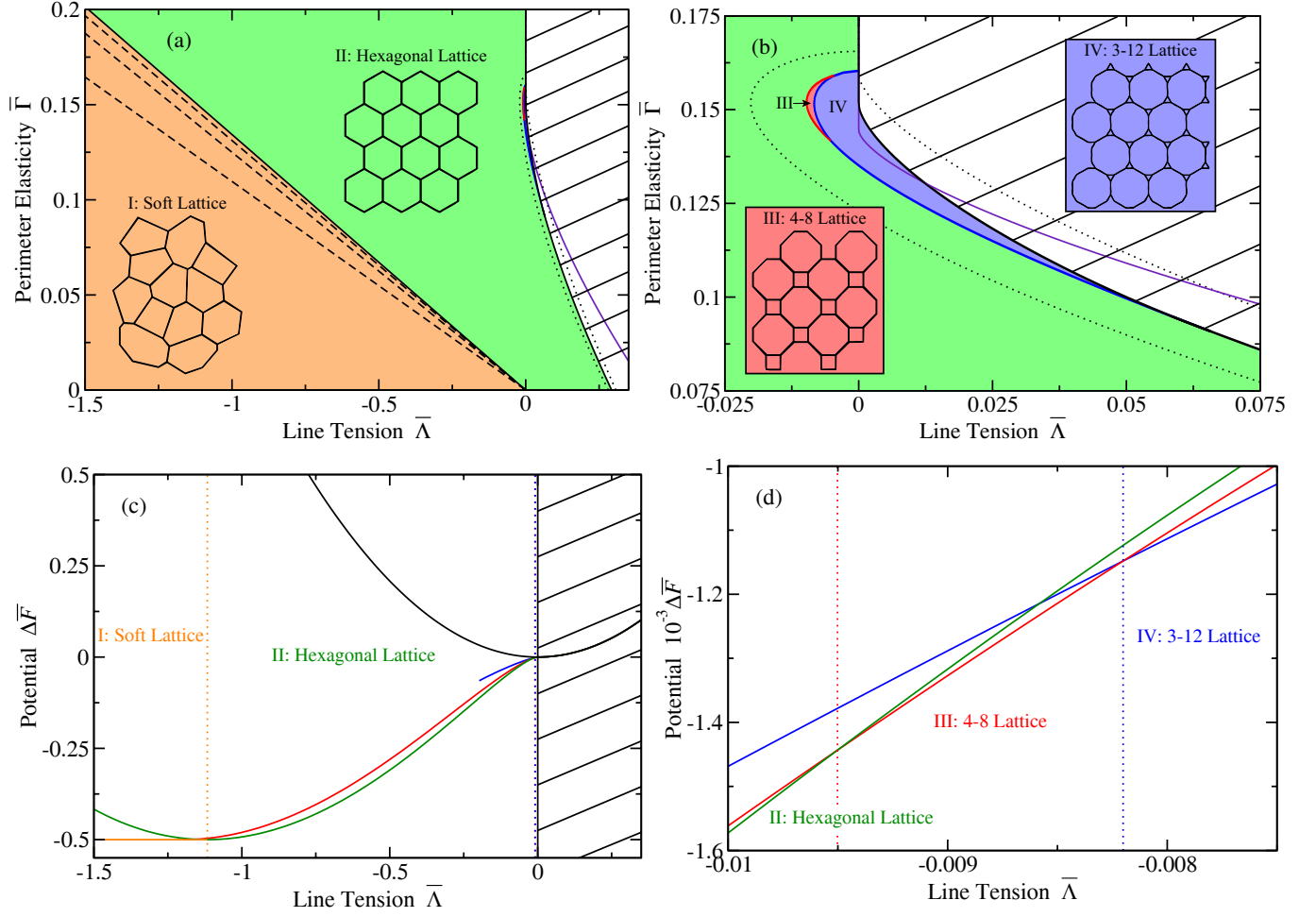


Fig. 2. (Colour on-line) (a) The ground-state diagram of the vertex model. In region I (orange) the ground states are degenerate and correspond to primarily irregular networks, in which all cells have equal perimeter $p = p_0$ and equal area $a = 1$. Within this region, dashed lines (described by eq. (7) for $n = 3, 4$, and 5) separate subregions with varying degrees of degeneracy. In these subregions the ground state is composed of irregular polygons with (from left to right) $n \geq 3$ sides, $n \geq 4$ sides, $n \geq 5$ sides, and $n = 6$ sides, respectively. The solid line separating region II where the regular hexagonal lattice is the ground state is described by eq. (7), with $n = 6$. Within the hatched region the ground state is a collapsed lattice of cells with zero area. (b) The region enclosed by the two dotted lines in (a) is magnified. Two additional regions III (red) and IV (blue) can be identified, where a “4-8” lattice and “3-12” lattice, respectively, have lower energies than the regular hexagonal lattice. The violet line indicates where the hexagonal lattice becomes locally unstable. In the region outside of the two dotted lines the nature of the ground state can be shown rigorously. (c) Diagrams of the potential energy per cell $\Delta\bar{F} = \bar{F} - e_0 - 1/2$ of different lattices, as a function of normalized line tension $\bar{\lambda}$ for $\bar{\Gamma} = 0.15$. Intersections of $\Delta\bar{F}$ for different lattices are marked by dotted lines. The lowest energy (orange) corresponds to soft lattices, which exist in region I for $\bar{\lambda} \lesssim -1.12$. The energy of the hexagonal lattice (green) has minimal energy in region II. The energy of collapsed lattices with zero area is indicated by the black line, and minimizes the energy in the hatched region. Furthermore, the energies of 4-8 and 3-12 lattices are indicated in red and blue, respectively. (d) Magnification of a small region of line tension of the energy diagram shown in (c), highlighting the regions where new periodic lattices have minimal energy.

If a cell has $a = 1$ and $p = p_0$, then the potential of that cell $e = e_0$ is at the absolute minimum of e for this cell.

First, we determine minimal potential configurations of single polygons. We then construct lower bounds of \bar{F} for arbitrary polygonal lattices and compare them to $\bar{F} = e_6$ for hexagonal lattices and to the value $\bar{F} = 1/2$ of a collapsed network ($a_\alpha = 0$, $p_\alpha = 0$). In this way we determine regions in parameter space where different types of ground-state networks exist, see fig. 2.

3.1 Polygons of minimal cell potential energy

First we determine the shapes that minimize the potential $e(a, p)$ of a single polygon with a fixed number of sides n . We identify several cases depending on the values of a and p , see table 1. An optimal polygon with $a > 0$ must obey $\partial e' / \partial \chi|_{\chi=1} = 0$, where

$$e' = \frac{1}{2} [(\chi^2 a - 1)^2 + \bar{\Gamma}(\chi p - p_0)^2 + e_0] \quad (5)$$

Table 1. Geometric constraints limit the values of the dimensionless perimeter p and area a that are possible for a polygonal cell. These constraints are listed in the rightmost column. Given a set of (a, p) (first and second columns), a corresponding polygon may or may not be a minimum of e , as indicated in the third column.

Perimeter	Area	Properties of $e(a, p)$	Geometric constraint on (a, p)
$p > p_0$	$a < 1$	potential minimum is a regular polygon	none
$p = p_0$	$a = 1$	this is the absolute potential minimum	$\bar{\Lambda} \leq -4\bar{\Gamma}\sqrt{n \tan(\pi/n)}$
$p = 0$	$a = 0$	potential minimum is a collapsed cell	$\begin{cases} \bar{\Lambda} \geq (2/c)[(2c - \bar{\Gamma})/3]^{3/2} & (\bar{\Gamma} < 2c) \\ \bar{\Lambda} \geq 0 & (\bar{\Gamma} \geq 2c) \end{cases}$
$p < p_0$	any a	potential can be reduced by increasing perimeter	none
$p = p_0$	$a \neq 1$	potential can be reduced by uniform scaling	none
$p > p_0$	$a \geq 1$	potential can be reduced by uniform compression	none

is the potential of a polygon rescaled by a factor $\chi = 1 + \epsilon$. This condition implies

$$2a(a - 1) + \bar{\Gamma}p(p - p_0) = 0. \quad (6)$$

Thus, we distinguish three cases of possible minima of e : i) $p < p_0$ and $a > 1$, ii) $p = p_0$ and $a = 1$, and iii) $p > p_0$ and $a < 1$. The first case i) is unstable with respect to shear, because $\partial e / \partial p|_a = \bar{\Gamma}(p - p_0) < 0$ and it is always possible to increase the perimeter of a polygon at fixed area. Case ii) corresponds to an absolute minimum of e , at which both area and perimeter take their preferred values. This is possible only if p_0 is larger than the minimal perimeter of an n -sided polygon of unit area, which leads to the condition

$$\bar{\Lambda} \leq -4\bar{\Gamma}\sqrt{n \tan\left(\frac{\pi}{n}\right)}. \quad (7)$$

In the limit of large n , eq. (7) becomes

$$\bar{\Lambda} < -4\sqrt{\pi}\bar{\Gamma}. \quad (8)$$

In case iii), the optimal shape is either a regular n -sided polygon or a collapsed cell ($a = 0$, $p = 0$). For $p > p_0$, $\partial e / \partial p|_a > 0$, thus reducing the perimeter at fixed area reduces the potential. A regular n -sided polygon has a smaller perimeter than any irregular n -sided polygon with equal area. Thus if $p > 0$ the optimal shape is a regular n -sided polygon. A special case is a collapsed cell with $a = 0$, $p = 0$, and $e = 1/2$. For regular polygons $a = cp^2$, where $c = \cot(\pi/n)/4n$. The potential is

$$e(p) = \frac{1}{2} [(cp^2 - 1)^2 + p\bar{\Lambda} + p^2\bar{\Gamma}], \quad (9)$$

the stationarity condition $de(p)/dp = 0$ provides the relation

$$4c^2p^3 + (2\bar{\Gamma} - 4c)p + \bar{\Lambda} = 0. \quad (10)$$

Combining eq. (10) with the equality $e > 1/2$, we obtain the condition for polygonal collapse:

$$\begin{aligned} \bar{\Lambda} &\geq \frac{2}{c} \left(\frac{2c - \bar{\Gamma}}{3} \right)^{3/2} & (\bar{\Gamma} < 2c), \\ &\geq 0 & (\bar{\Gamma} \geq 2c). \end{aligned} \quad (11)$$

In the limit of large n , eq. (11) becomes

$$\begin{aligned} \bar{\Lambda} &\geq \frac{8}{\sqrt{\pi}} \left(\frac{1 - 2\pi\bar{\Gamma}}{3} \right)^{3/2} & (2\pi\bar{\Gamma} < 1), \\ &\geq 0 & (2\pi\bar{\Gamma} \geq 1). \end{aligned} \quad (12)$$

Note that, as shown in sect. 3.2, eq. (7) and eq. (11) define characteristic boundary lines in the ground-state diagram of the vertex model, see fig. 2a.

3.2 Networks of minimal potential

In sect. 3.1 we showed that the potential energy $e(a, p)$ of an individual cell is minimized by regular n -sided polygons. Here we determine ground-state networks, defined as the configurations of polygons that minimize the potential \bar{F} for a given set of parameter values $\bar{\Lambda}$ and $\bar{\Gamma}$ with periodic boundary conditions. The size of the periodic box is also varied in the minimization. This minimization problem is solved by using the minimal-energy polygons described in the last section together with the fact that the average neighbour number is less than or equal to six. Note that in periodic networks containing only threefold vertices the average neighbour number is exactly six. In periodic networks containing manifold vertices, the average neighbour number is less than six. Details of the determination of ground states and the corresponding ground-state diagram are presented in appendix A.

In figs. 2a and b we present the ground-state diagram of the vertex model. We find four distinct regions of parameter space ($\bar{\Lambda}$ and $\bar{\Gamma}$): I irregular networks are the (degenerate) ground states, II the ground state is a hexagonal lattice, and two further regions, III and IV, where other periodic lattices are the ground state. In the hatched region the ground state is a collapsed network of cells with zero area. Region I is bounded by a straight line described by eq. (7) for $n = 6$. Region I can be further divided into four subregions (separated by dashed lines in fig. 2a), characterized by the degree of degeneracy of the ground states. From right to left the ground states in the four subregions are composed of irregular n -sided polygons with $n = 6$, $n \geq 5$, $n \geq 4$, and all n , respectively. They are obtained

from eq. (7) for $n \leq 6$. The region inside of the dotted lines is highlighted in fig. 2b. Outside of this region, the state diagram is known exactly, see appendix A. The dotted line within the hatched region is given by eq. (12), while the dotted line within region II is determined in appendix A. Between these dotted lines we find two small regions III (red) and IV (blue) where two new periodic lattices have a lower energy than the hexagonal lattice, see fig. 2. These regions were identified numerically by comparing the minimized energies of various periodic tilings of the plane. Furthermore, we show in fig. 2b a violet line, showing the limit of local stability of the hexagonal network.

The energy of different periodic network configurations is shown in figs. 2c and d as a function of $\bar{\Lambda}$ for $\bar{\Gamma} = 0.15$. The energy of soft lattices in region I is constant and the corresponding line (orange) exists for $\bar{\Lambda} \lesssim -1.12$, up to the dotted line in fig. 2c. The energy of hexagonal lattices is indicated in green, while those of periodic “4-8” and “3-12” lattices are shown in red and blue, respectively. Note that the blue line only exists for $\bar{\Lambda} \gtrsim -0.20$. The black line shows the energy of collapsed cells of zero area. The energy branch of soft lattices (orange) meets the energy of the hexagonal lattice (green) at a point where the energy of the hexagonal lattice has zero slope, indicative of a second-order transition, see fig. 2c. The transitions between regions II, III, and IV, however, are first-order transitions because the different branches have different slopes, see fig. 2d.

4 Elastic properties: Shear and compression moduli

Here we discuss the shear and compression moduli of the ground states of the vertex model. For fixed cell number N and box dimensions L_x and L_y , we define the minimum of the potential F by the function $F(L_x, L_y)$. The shear modulus μ can then be obtained as

$$\mu = \frac{1}{2A} \frac{\partial^2 F(L_x, L_y)}{\partial \gamma^2} \Big|_{\gamma=0}, \quad (13)$$

where $A = L_x L_y$, $L_x = L_x^{(0)}(1 + \gamma)$, and $L_y = L_y^{(0)}/(1 + \gamma)$. Here, $L_x^{(0)}$ and $L_y^{(0)}$ define the size of a reference box and γ is a dimensionless rescaling parameter. Similarly, the compression modulus λ can be obtained as

$$\lambda = \frac{1}{4A} \frac{\partial^2 F(L_x, L_y)}{\partial \epsilon^2} \Big|_{\epsilon=0}, \quad (14)$$

where $L_x = L_x^{(0)}(1 + \epsilon)$ and $L_y = L_y^{(0)}(1 + \epsilon)$. In the region where the ground state is a hexagonal lattice the network has both nonzero shear and compression moduli

$$\begin{aligned} \bar{\mu} &= (\sqrt{3}/16)p^2 + 2\sqrt{3}\bar{\Gamma} - 1/2, \\ \bar{\lambda} &= 6\sqrt{3}\bar{\Gamma} + 3\sqrt{3}\bar{\Lambda}/p, \end{aligned} \quad (15)$$

where $\bar{\lambda} = \lambda/(KA_0)$ and $\bar{\mu} = \mu/(KA_0)$.

As line tension and perimeter elasticity are reduced, the shear modulus of the network decreases; when the equilibrium perimeter of cells in the hexagonal ground state reaches $p = p_0$ the shear modulus vanishes, yielding a transition line at $\bar{\Lambda} = -2^{5/2}3^{1/4}\bar{\Gamma}$. This is exactly the transition line where the ground state changes from a network of regular hexagons to a degenerate network where all cells have $a = 1$, $p = p_0$, and $e = e_0$, see sect. 3.2. For line tensions and perimeter elasticity below this transition line, small shear deformations can be performed with no work required, indicative of a transition from a solid to a soft network.

For sufficiently high perimeter elasticity and tension the compression modulus vanishes. Setting $\lambda = 0$ in eq. (15) yields an instability line for the hexagonal lattice

$$\begin{aligned} \bar{\Lambda} &= 2^{3/2}3^{-5/2}(\sqrt{3} - 12\bar{\Gamma})^{3/2} & (\bar{\Gamma} < \sqrt{3}/12), \\ &= 0 & (\bar{\Gamma} \geq \sqrt{3}/12). \end{aligned} \quad (16)$$

This line lies primarily in the hatched region of the state diagram, see the violet line in fig. 2. For points in the phase diagram beyond this line hexagonal networks are unstable.

5 Topological changes

The ground state is an important reference state for cellular networks, representing the most relaxed configuration. Network configurations that correspond to cell packings in tissues in general do not correspond to ground states. Active processes such as cell division and morphogenetic movements perform mechanical work, and thus generate network configurations that are of higher potential energy than the ground state. However, these configurations are force-balanced, and thus local minima of the potential F [3]. The large number of such local minima are physiologically relevant, and are generated via topological rearrangements of the network. Such topological changes are often associated with energy barriers. We discuss two types of topological transitions called T1 and T2 transitions [28]. A T1 transition occurs when a cell boundary shrinks to zero length, forming a fourfold vertex, which subsequently decomposes, creating a new cell bond. This process changes neighbourhood relationships, see fig. 3. A T2 transition occurs when a n -sided polygon shrinks to a point and is replaced with an n -fold vertex, see fig. 4. Such a T2 transition corresponds to cell extrusion from an epithelium, typically associated with cell death (apoptosis).

5.1 Cell extrusion by T2 transitions

Cell extrusion can be discussed in a simple scenario where triangular cells of dimensionless side length $\ell = l/\sqrt{A_0}$ are introduced at the vertices of a hexagonal network. The resulting lattice consists of three- and twelve-sided cells, as in region IV of fig. 2. We show in fig. 5 the potential energy per cell of the lattice as a function of the side length

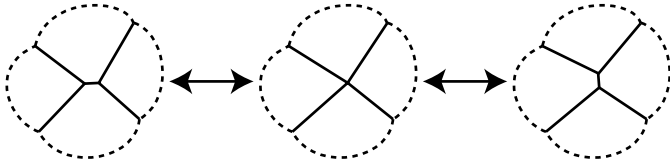


Fig. 3. Schematic of a network rearrangement called a T1 transition. Two threefold vertices combine to form a fourfold vertex, which subsequently decomposes into two new threefold vertices. The overall topology of the network is changed during this process, and cells change their neighbourhood relation.

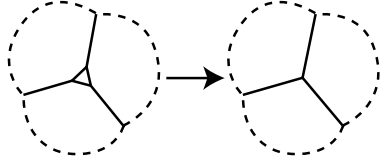


Fig. 4. Schematic of a network rearrangement called a T2 transition. A cell shrinks to zero area and is removed from the lattice. This process corresponds to the extrusion of a cell from an epithelium (apoptosis).

ℓ of the triangles. Depending on parameter values we find three distinct behaviours: (a) instability of triangles with respect to spontaneous cell extrusion, (b) locally stable triangles with a barrier to cell extrusion, and (c) globally stable triangles in region IV of fig. 2.

5.2 Energetics of manifold vertices

The energetics of manifold vertices in the vertex model are relevant for the dynamics of boundary rearrangements, *i.e.* T1 transitions. A manifold vertex is unstable if there exists a decomposition into infinitesimally separated threefold vertices that lowers the potential F of the network. For example, a fourfold vertex can be replaced with two threefold vertices in two topologically different ways, see fig. 3. Our work suggests that manifold vertices are unstable if all cells are equivalent (common values of A_0 , A , Γ , and K), unless $a = 1$ and $p = p_0$. A general proof of this statement is lacking, but it holds true for any case investigated.

Consider for example the case where cells meeting at a fourfold vertex have equal area $a \neq 1$ and equal perimeter $p \neq p_0$. If a fourfold vertex decomposes into two threefold vertices then the total energy change is

$$\delta\bar{F} = \frac{1}{N} \sum_{\alpha} [(a_{\alpha} - 1)\delta a_{\alpha} + \bar{\Gamma}(p_{\alpha} - p_0)\delta p_{\alpha}], \quad (17)$$

plus terms of order δa_{α}^2 and δp_{α}^2 . Substituting $a_{\alpha} = a$ and $p_{\alpha} = p$, eq. (17) reduces to

$$\delta\bar{F} = \frac{\bar{\Gamma}(p - p_0)}{N} \sum_{\alpha} \delta p_{\alpha}. \quad (18)$$

Thus the change in potential during decomposition of a fourfold vertex is proportional to the total perimeter

change in this case. There are two topologically distinct ways to decompose a fourfold vertex into two threefold vertices, see fig. 3. For each of these two topologically distinct decompositions, there is a continuum of possible variations, assuming that infinitesimal movements of the resulting threefold vertices are permitted. As a consequence, there always exist many decompositions of a fourfold vertex into threefold vertices, some of which increase and some of which decrease the total perimeter. Thus it is possible to lower the potential of the network by decomposing the fourfold vertex, and the fourfold vertex is always unstable in this case. Finally, if cells are unequal in their mechanical properties then stable manifold vertices can occur.

6 Cell division and tissue growth

Thus far we have defined the ground states of the vertex model and discussed topological processes necessary for the analysis of physiologically relevant states, see sects. 3 and 5. Here we exposit quasistatic algorithms that describe cell division and tissue growth in the vertex model.

6.1 Cell division in the vertex model

In the vertex model, cell division can be introduced by the following steps [3] (algorithm I): i) Initially the network is in a force-balanced state, *i.e.* a local minimum of F . ii) A cell α is selected to divide. iii) The preferred area $A_{\alpha}^{(0)}$ of cell α is doubled quasistatically. iv) A new cell boundary is introduced bisecting the cell α into two daughter cells. In the case of isotropic cell division, the new cell bond has a random orientation. We choose it to pass through the center of cell α , defined as the average of the vertex positions of that cell. v) The preferred areas $A_{\alpha}^{(0)}$ of the daughter cells are reset to the original preferred area of cells. vi) The system is relaxed to a force-balanced configuration¹. This relaxation introduces network rearrangements by T1 and T2 transitions. A detailed discussion of the algorithms used to account for topological changes are given in appendix B.

For simplicity and to improve computational performance, the steps described above can be reduced as follows (algorithm II): i) Initially the network is in a force-balanced state. ii) A cell α is selected to divide. iii) The cell α is bisected into two daughter cells by inserting a new cell bond. This new cell bond has a random orientation and passes through the geometric center of cell α . iv) The system is relaxed to a force-balanced state. We show in appendix C that algorithm I and II give very similar results, and that for practical purposes algorithm II is sufficient to describe tissue morphology.

¹ Both here and in ref. [3] force-balanced states are obtained using the Polak-Ribière variant of the conjugate gradient algorithm [29], *e.g.*, as implemented in the GNU Scientific Library [30].

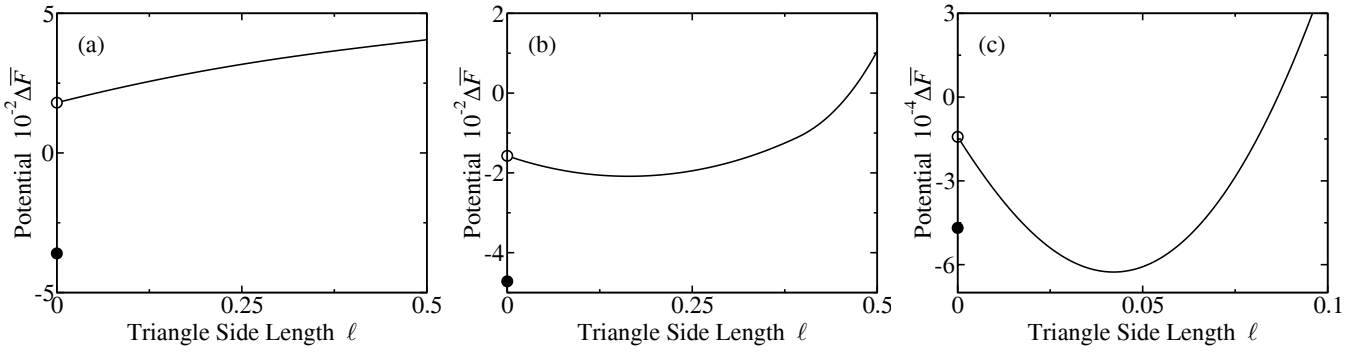


Fig. 5. Diagrams of the potential energy per cell $\Delta\bar{F} = \bar{F} - e_0 - 1/2$ of “3-12” lattices, which are hexagonal lattices into which triangular cells are periodically introduced, see fig. 2b. Different parameter values reveal three possible situations: (a) no barrier to cell extrusion, (b) a finite barrier to cell extrusions and (c) stable 3-12 lattices in region IV. Parameter values are $(\bar{A}, \bar{T}) = (0.12, 0.04)$, $(0, 0.1)$, and $(-0.005, 0.15)$, corresponding to (a), (b), and (c), respectively.

6.2 Tissue morphologies generated by growth

Growth simulations are performed by randomly selecting cells with equal probability to divide. A single cell division is performed using algorithm II and the next cell is subsequently selected at random. This implies a quasistatic representation of growth. This process can be related to real time by assigning times to each cell division event. This can be done such that the probability per unit time of each cell to divide, the cell division rate k_d , is constant. Alternatively, one can describe the process as a function of generation number $g = \log_2(N/N_0)$, where N is the cell number and N_0 is the cell number in the original generation of cells.

We show in fig. 6a polygon class distributions resulting from vertex model simulations using algorithm II (solid line). These data were obtained by performing 10^4 simulations, each starting from 16 cells and having 10^2 subsequent cell divisions. The errors are smaller than the line width and are thus not indicated. Note that neighbor numbers in the simulations were determined without a cutoff for minimal bond length and therefore the average neighbor number is 6. This data is compared to experimental estimates of neighbor number distributions in the developing wing of fruit fly *Drosophila* (data from ref. [3]).

In a series of studies spanning from 1928 to 1950, F.T. Lewis reported an approximately linear relationship between the number of sides and the area of cells of various organisms [31,32]. This maxim is commonly referred to as Lewis’s Law. We present in fig. 6b the area of polygons resulting from simulated growth in the vertex model (algorithm II, solid line) and values reported experimentally (dashed line). Note that our simulations show that the average area exhibits nonlinear behavior. However, if the same data were presented over a limited range of n (e.g., $4 \leq n \leq 8$) and with larger error bars, then one might mistakenly identify a linear relationship. Nonlinearities can have several causes, for instance because cells cannot have arbitrarily large areas while the number of neighbors can become large. These nonlinearities are accessible in simulations, where precise statistics are pos-

sible. Lewis’s Law therefore represents an approximation that is valid for limited ranges of n .

We also present in figs. 6c and d the full distributions of polygon area and perimeter. The mean areas $\langle a \rangle_n$ presented in fig. 6b are the first moments of the distributions shown in 6c.

7 Conclusions

In ref. [3], a vertex model was shown to reproduce morphology and topology of epithelial network configurations in the developing wing of the fruit fly. Similar approaches have subsequently been employed to study a variety of biological problems including wound closure [7,26], cell sorting [8], and the mechanical regulation of cell division and growth [9]. Here we discuss key properties of these vertex models.

We showed in sect. 3 and the accompanying appendix A that ground states of the vertex model can be determined analytically for most parameter values (\bar{A}, \bar{T}) . This was done by reformulating the vertex model in terms of isolated polygons (sect. 3.1). The full phase diagram is presented in fig. 2. Using this phase diagram we identify transition lines related to shear and compression moduli of the bulk tissue.

While the ground state is an important reference state, active processes such as cell division and death result in irregular networks that correspond to local minima in the vertex model. In order to understand physiologically relevant states, it is first necessary to understand the relevant topological processes that can occur. We show that a simplified algorithm, which omits quasistatic doubling of preferred area, is sufficient to describe cell packings in growing epithelia. Furthermore, we investigate details concerning topological network rearrangements by T1 and T2 transitions, in sect. 5. We find that processes including cell extrusion and cell boundary rearrangements can involve energetic barriers in the vertex model.

The vertex model investigated here provides a basis to describe quasistatic remodeling of epithelia during development. Additional cell properties and molecular signaling

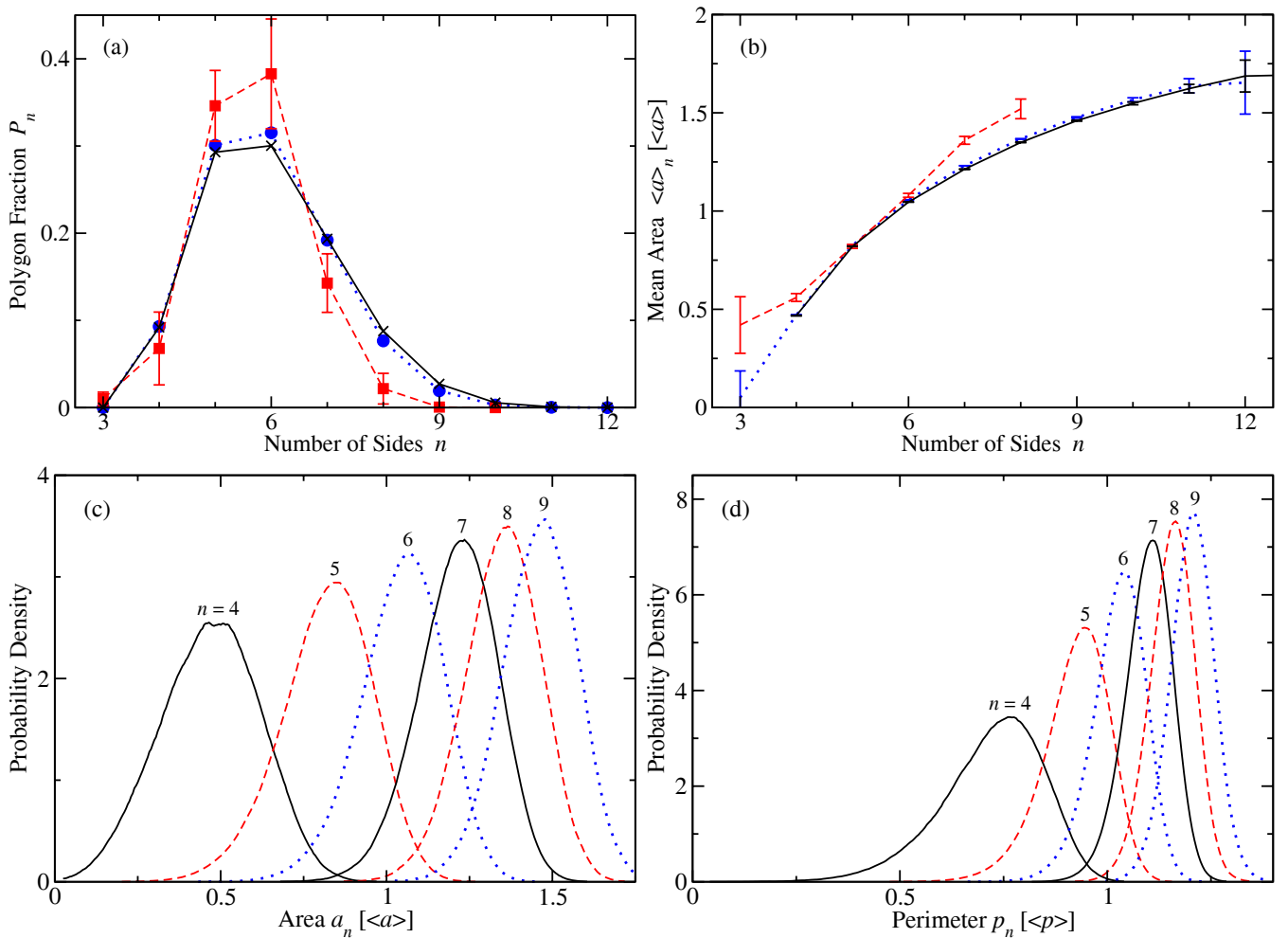


Fig. 6. (Colour on-line) (a) Fraction of n -sided polygons as a function of cell neighbour number n . Neighbour number distributions are obtained in growth simulations with algorithm II for $(\bar{\Lambda}, \bar{\Gamma}) = (0.12, 0.04)$ without a length cutoff (black) and with a length cutoff of 20% of the average bond length (blue). Experimental data (red) of the wing of the fruit fly from ref. [3] is shown for comparison. The length cutoff defines a distance, below which two threefold vertices are considered to be a single fourfold vertex. For each polygon containing one or more edges shorter than the length cutoff, the neighbour number n is reduced appropriately. (b) Average area of n -sided polygons, normalized by the average area of cells in the network, for the same simulations and experiments shown in (a). (c) Stationary probability distributions of the areas of n -sided polygons in the growth simulations with algorithm II that are indicated by solid lines in (a) and (b). (d) Stationary probability distributions of the perimeters of n -sided polygons in the simulations shown in (c).

processes can be naturally incorporated in this theoretical framework. This opens the possibility to study the interplay of active mechanics and cellular signaling in the shaping and patterning of tissues.

Appendix A. Ground states of the vertex model

Appendix A.1. Networks of identical cells

We first determine the ground state of networks of identically shaped cells. Networks of identically shaped cells can only be n -sided polygons with $n = 3, 4, 5$ or 6 . Note that, due to the restriction of average neighbour number, networks of identically shaped cells with $n = 3, 4$ or 5

must contain fourfold or manyfold vertices. As shown in sect. 3.1, for $\bar{\Lambda} < -2^{5/2}3^{1/4}\bar{\Gamma}$ the lowest potential energy of individual polygons corresponds to irregular polygons with preferred area and perimeter. Similarly, it was shown that if

$$\bar{\Lambda} \geq 2 \cdot 3^{-5/2}(\sqrt{3} - 12\bar{\Gamma})^{3/2} \quad (\bar{\Gamma} < \sqrt{3}/12), \quad (\text{A.1})$$

or

$$\bar{\Lambda} \geq 0 \quad (\bar{\Gamma} \geq \sqrt{3}/12), \quad (\text{A.2})$$

then the lowest potential of individual polygons corresponds to collapsed cells with $a = 0$. These results also apply for networks of identical polygons. For values of $\bar{\Lambda}$ between these two cases, a regular hexagon of minimal e has a lower potential than any other n -sided polygon with

Table 2. Ground states of the potential energy \bar{F} of networks of identically shaped cells as a function of the dimensionless line tension $\bar{\Lambda}$ and perimeter elasticity $\bar{\Gamma}$. For $\bar{\Lambda} < -2^{5/2}3^{1/4}\bar{\Gamma}$ the ground states are degenerate, consisting of identical irregular polygons with $a = 1$ and $p = p_0$.

Parameter values		Ground state (identical cells)
$\bar{\Lambda} < -2^{5/2}3^{1/4}\bar{\Gamma}$	–	irregular polygons ($a = 1, p = p_0$)
$-2^{5/2}3^{1/4}\bar{\Gamma} \leq \bar{\Lambda} < 2 \cdot 3^{-5/2}(\sqrt{3} - 12\bar{\Gamma})^{3/2}$	$\bar{\Gamma} < \sqrt{3}/12$	} hexagonal lattice
$-2^{5/2}3^{1/4}\bar{\Gamma} \leq \bar{\Lambda} < 0$	$\bar{\Gamma} \geq \sqrt{3}/12$	
$\bar{\Lambda} \geq 2 \cdot 3^{-5/2}(\sqrt{3} - 12\bar{\Gamma})^{3/2}$	$\bar{\Gamma} < \sqrt{3}/12$	} collapsed lattice ($a = 0, p = 0$)
$\bar{\Lambda} \geq 0$	$\bar{\Gamma} \geq \sqrt{3}/12$	

$n \leq 6$. Interestingly, for $\bar{\Lambda} \geq 0$ this fact also follows directly from the so-called ‘‘Honeycomb Conjecture’’, which states that a network of regular hexagons has the smallest perimeter of any periodic tiling of equal area regions [33]. These arguments define the ground states of networks of identical cells, depending on the values of $\bar{\Lambda}$ and $\bar{\Gamma}$, see table 2.

Appendix A.2. General networks of cells

We now consider all possible networks and determine the ground states of \bar{F} . For $\bar{\Lambda} < -2^{5/2}3^{1/4}\bar{\Gamma}$ any state for which all cells have area $a = 1$ and perimeter $p = p_0$ is a ground state of the system. In the following we only consider parameter values with $\bar{\Lambda} \geq -2^{5/2}3^{1/4}\bar{\Gamma}$.

The ground state of all networks composed of n -sided polygons with $n \leq 6$ is a perfect hexagonal network with optimized areas. This follows because an optimal hexagon has a lower potential than any other n -gon with $n \leq 6$. The problem is nontrivial in the case where some polygons have $n > 6$ sides. Because for periodic boundary conditions the average neighbor number $\langle n \rangle$ in an arbitrary network is $\langle n \rangle \leq 6$, any n -gon with $n > 6$ must be balanced by a number of n -gons with $n < 6$. We use this fact to determine a lower bound $\Delta_{\text{net}}(n) + e_6$ of the potential of networks containing cells with $n > 6$, where e_6 denotes the optimal energy of regular hexagons.

For a network containing an $n > 6$ -sided cell, the average neighbour number can be less than or equal to 6 if the network also contains $n - 6$ pentagons, $(n - 6)/2$ quadrilaterals, or $(n - 6)/3$ triangles. Combinations of triangles, quadrilaterals, and pentagons are also possible. A lower bound on the potential difference between such a network and one containing only regular hexagons is given by

$$\Delta_{\text{net}}(n) = \Delta_n + (n - 6) \min \left[\Delta_5, \frac{\Delta_4}{2}, \frac{\Delta_3}{3} \right], \quad (\text{A.3})$$

where $\Delta_n = e_n - e_6$. Here e_n is the lowest energy e of an n -sided polygon given $\bar{\Lambda}$ and $\bar{\Gamma}$. Note that as shown in sect. 3.1, the corresponding optimal polygon shape is either a regular n -sided polygon, an irregular polygon with $a = 1$ and $p = p_0$, or a collapsed cell ($a = 0, p = 0$). If $\Delta_{\text{net}}(n) > 0$, then any network constructed using cells with six or fewer sides together with cells with $n > 6$ sides will have a higher potential than the hexagonal lattice. If

$\Delta_{\text{net}}(n) > 0$ for all $n > 6$, then the optimal hexagonal network is the ground state of the system for the given parameter values. We note that e_n is monotonically decreasing with n , so that

$$\Delta_{\text{net}}(n') \geq \Delta_{\text{net}}(n) + e_\infty - e_n, \quad (\text{A.4})$$

for all $n' \geq n$, where

$$e_\infty = \lim_{n \rightarrow \infty} e_n. \quad (\text{A.5})$$

The procedure for showing that the hexagonal lattice is the ground state for a particular set of parameter values $(\bar{\Lambda}, \bar{\Gamma})$ is as follows. Starting at $n = 7$, we check the inequality $\Delta_{\text{net}}(n) > 0$ for increasing values of n . If $\Delta_{\text{net}}(n) < 0$ for any n , the then hexagonal network may not be the ground state. If for $\Delta_{\text{net}}(n) > 0$ we also find $\Delta_{\text{net}}(n) + e_\infty - e_n > 0$ then the hexagonal network is proven to be the ground state, and larger n do not need to be considered. We continue checking these two inequalities for increasing values of n , until either $\Delta_{\text{net}}(n) < 0$ for some n , and no conclusions can be drawn, or $\Delta_{\text{net}}(n) + e_\infty - e_n > 0$, and thus the hexagonal lattice is shown to be the ground state.

We have applied these arguments numerically at each set of parameter values $(\bar{\Lambda}, \bar{\Gamma})$ in the ranges $-1.5 \leq \bar{\Lambda} \leq 0.5$, $0 \leq \bar{\Gamma} \leq 0.2$ in increments of $\Delta\bar{\Lambda} = \Delta\bar{\Gamma} = 10^{-4}$. We find that the hexagonal lattice is the ground-state network of the vertex model everywhere in the part of region II of figs. 2a and b that is exterior to the dotted lines.

Appendix B. Topological changes during network relaxation

When the potential energy F is minimized by a conjugate gradient procedure, a cell bond can shrink to zero length and the network can undergo a T1 transition. Similarly, a cell can shrink to zero area and induce a T2 transition.

Appendix B.1. T1 transitions

Method A. Each bond $\langle i, j \rangle$ is assigned a state variable $\sigma_{\langle i, j \rangle}$, which can take the values 0 or 1. Initially $\sigma_{\langle i, j \rangle} = 1$ for all bonds. The algorithm consists of the following steps,

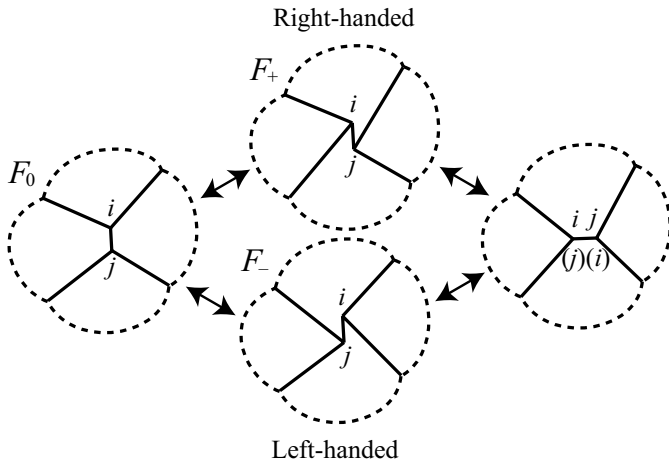


Fig. 7. Schematic representation of T1 transitions as implemented in the numerical algorithm described in appendix B.

applied at each iteration of energy minimization: i) A T1 transition is performed whenever a bond with $\sigma_{\langle i,j \rangle} = 1$ shrinks below a cutoff length l_{\min} , *i.e.* if $l_{ij} < l_{\min}$. After the transition this bond no longer exists, and the newly created bond is assigned $\sigma_{\langle i,j \rangle} = 0$. ii) For all bonds with $l_{ij} \geq l_{\min}$ we set $\sigma_{\langle i,j \rangle} = 1$.

Method B is the algorithm used in ref. [3]. The algorithm consists of the following steps, applied at each iteration of energy minimization: i) For each bond with $l_{ij} < l_{\min}$ we determine F_+ and F_- , the energies corresponding to network configurations due to right-handed and left-handed T1 transitions, see fig. 7. ii) The network with the lowest potential value F_0 , F_+ , or F_- is chosen, where F_0 is the energy of the initial network, see fig. 7. This implies that a T1 transition occurs whenever F_+ or F_- is below F_0 .

Method C is similar to Method B, except that F_+ and F_- are determined after an additional relaxation, which keeps all vertices fixed except for i and j .

We find that polygon distributions and cell area variations are indistinguishable for tissues obtained using these three algorithms (data not shown). The simplest algorithm presented here (Method A) is more robust to numerical implementation than methods B and C, because methods B and C require precise computation of small potential changes $F_+ - F_0$ and $F_- - F_0$.

Appendix B.2. T2 transitions

T2 transitions are accounted for by replacing a cell α with $A_\alpha < A_{\min}$ with a vertex, where A_{\min} is an area cutoff.

Appendix C. Comparison of growth algorithms

Algorithm II for quasistatic cell division introduced in this paper is a simplified version of Algorithm I, which was

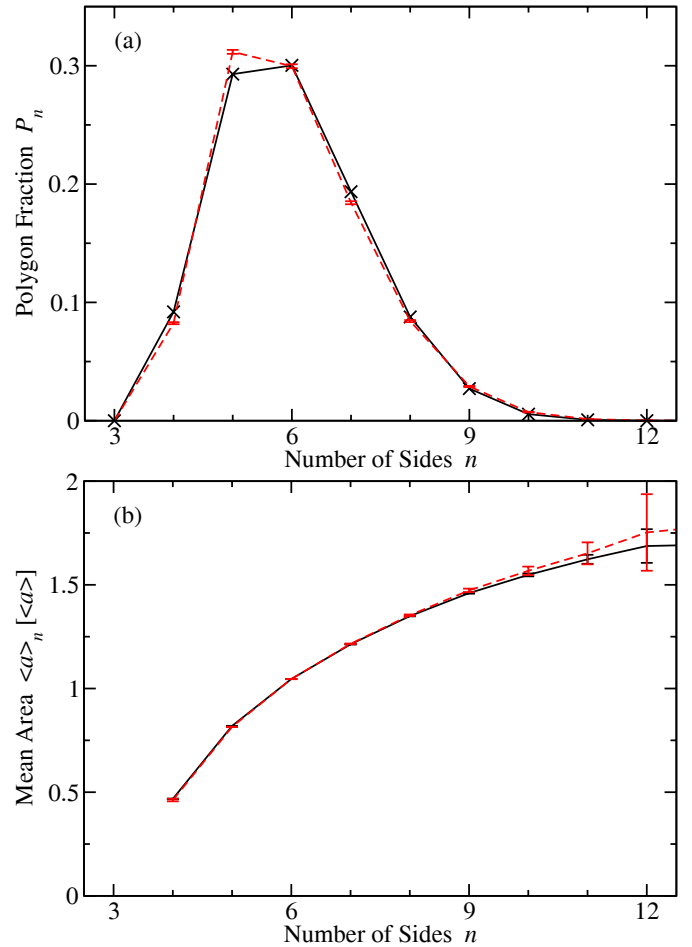


Fig. 8. (Colour on-line) Comparison of algorithms I (dashed red lines) and II (solid black lines), which use different rules for cell division, for $(\bar{A}, \bar{T}) = (0.12, 0.04)$. (a) Fraction of n -sided polygons as a function of cell neighbour number n . (b) Average area of n -sided polygons, normalized by the average area of the network, for the same simulations shown in (a). The solid black lines in (a) and (b) are the same as in figs. 6a and b.

used in ref. [3], see sect. 6.1. We show in fig. 8 that these two growth algorithms give very similar results (compare solid and dashed lines).

Note that the polygon distributions shown in ref. [3] differ slightly from the dashed line in fig. 8, which is obtained using the same algorithm. Reasons for this are: i) A length cutoff was used when defining neighbour numbers in ref. [3], which is necessary when comparing with experiment. No such cutoff is used here. ii) In ref. [3] a single network containing 10^4 cells was used, whereas here we use 10^3 networks (dashed line in fig. 8) and 10^4 networks (solid line) containing ~ 110 cells each. This implies a larger statistical error in ref. [3] compared to fig. 8. iii) There are additional numerical inaccuracies in ref. [3].

R.F., J.-C.R., B.A., S.E., and F.J. were supported by the Max Planck Gesellschaft. D.B.S. acknowledges NSERC and the DAAD. D.B.S. thanks Peer Mumcu for discussions.

References

1. M.C. Gibson, A.B. Patel, R. Nagpal, N. Perrimon, *Nature* **442**, 1038 (2006).
2. R. Nagpal, A. Patel, M.C. Gibson, *BioEssays* **30**, 260 (2008).
3. R. Farhadifar, J.C. Röper, B. Aigouy, S. Eaton, F. Jülicher, *Curr. Biol.* **17**, 2095 (2007).
4. T. Nagai, K. Kawasaki, K. Nakamura, *J. Phys. Soc. Jpn.* **57**, 2221 (1988).
5. M. Weliky, G. Oster, *Development* **109**, 373 (1990).
6. T. Nagai, H. Honda, *Philos. Mag. B* **81**, 699 (2001).
7. T. Nagai, H. Honda, *Phys. Rev. E* **80**, 061903 (2009).
8. K.P. Landsberg, R. Farhadifar, J. Ranft, D. Umetsu, T.J. Widmann, T. Bittig, A. Said, F. Jülicher, C. Dahmann, *Curr. Biol.* **19**, 1950 (2009).
9. T. Aegerter-Wilmsen, A.C. Smith, A.J. Christen, C.M. Aegerter, E. Hafen, K. Basler, *Development* **137**, 499 (2010).
10. B. Aigouy, R. Farhadifar, D.B. Staple, A. Sagner, J.C. Röper, F. Jülicher, S. Eaton, *Cell* **142**, 773 (2010).
11. J. Plateau, *Statique expérimentale et théorique des Liquides soumis aux seules Forces moléculaires* (Paris, Gauthier-Villars; London, Trübner & Co.; Gand and Leipzig, F. Clemm, 1873).
12. J.E. Taylor, *Ann. Math.* **103**, 489 (1976).
13. K. Kawasaki, T. Nagai, K. Nakashima, *Philos. Mag. B* **60**, 399 (1989).
14. K. Nakashima, T. Nagai, K. Kawasaki, *J. Stat. Phys.* **57**, 759 (1989).
15. T. Okuzono, K. Kawasaki, *Phys. Rev. E* **51**, 1246 (1995).
16. R.L. Fullman, in *Metal Interfaces* (American Society for Metals, Cleveland, 1952) pp. 179–207.
17. A. Soares, A.C. Ferro, M.A. Fortes, *Scr. Met.* **19**, 1491 (1985).
18. D. Weaire, *The Physics of Foams* (Oxford University Press, 2000) ISBN 0198505515.
19. F. Graner, J.A. Glazier, *Phys. Rev. Lett.* **69**, 2013 (1992).
20. J.C.M. Mombach, R.M.C. de Almeida, J.R. Iglesias, *Phys. Rev. E* **48**, 598 (1993).
21. R. Smallwood, *Wiley Interdiscip. Rev. Syst. Biol. Med.* **1**, 191 (2009).
22. P. Pathmanathan, J. Cooper, A. Fletcher, G. Mirams, P. Murray, J. Osborne, J. Pitt-Francis, A. Walter, S.J. Chapman, *Phys. Biol.* **6**, 036001 (2009).
23. Y. Hatwalne, S. Ramaswamy, M. Rao, R.A. Simha, *Phys. Rev. Lett.* **92**, 118101 (2004).
24. K. Kruse, J.F. Joanny, F. Jülicher, J. Prost, K. Sekimoto, *Eur. Phys. J. E* **16**, 5 (2005).
25. T. Bittig, O. Wartlick, A. Kicheva, M. González-Gáitan, F. Jülicher, *New J. Phys.* **10**, 063001 (2008).
26. M.S. Hutson, J. Veldhuis, X. Ma, H.E. Lynch, P.G. Cranston, G.W. Brodland, *Biophys. J.* **97**, 3075 (2009).
27. S. Hilgenfeldt, S. Erisken, R.W. Carthew, *Proc. Natl. Acad. Sci. U.S.A.* **105**, 907 (2008).
28. D. Weaire, N. Rivier, *Contemp. Phys.* **25**, 59 (1984).
29. E. Polak, G. Ribière, *Rev. Fr. Inform. Rech. Oper.* **3**, 35 (1969).
30. B. Gough, *GNU Scientific Library Reference Manual*, 3rd edition (Network Theory Limited, 2009) ISBN 0954612078.
31. F.T. Lewis, *Anat. Rec.* **38**, 341 (1928).
32. F.T. Lewis, *Am. J. Botany* **30**, 766 (1943).
33. T.C. Hales, *Discrete Comput. Geom.* **25**, 1 (2001).